Geoscience Letters

RESEARCH LETTER

Open Access

An intensity index and its application for summertime extratropical cyclones in East Asia

Sitao Wang[1], Yujing Qin[1*], Chuhan Lu[2*] and Zhaoyong Guan[1]

Abstract

The intensity definition and classification of the extratropical cyclone (EC) are still less studied than the tropical cyclone, due to the relatively ambiguous structure and diverse life cycle of ECs. In this study, a two-dimensional objective cyclone identification method based on outermost closed isolines is used to obtain the EC-related datasets, and the summertime ECs in East Asia are classified by the relationship between ECs of different intensities and the corresponding precipitation. The results show that compared with the cyclone mean depth, central wind and other traditional intensity indicators, the cyclone intensity index that is the maximum product of the EC-associated wind speed and specific humidity, has the highest correlation with the EC-associated maximum precipitation ($r = 0.74$). To simplify the definition of cyclone intensity index, the vq_{max} within the radius of 300 km from the cyclone center is defined as the cyclone intensity. According to the relationship between EC and precipitation intensity and the precipitation grades in China, the ECs in East Asia are classified into four levels. Accordingly, the EC-associated maximum precipitation increases substantially with the raising of cyclone level. In particular, 32.8% of heavy rain events in East Asia in summer are related to ECs of the strongest category. The results will facilitate a better understanding of the relationship between the strongest category EC and local precipitation.

Keywords Extratropical cyclone, Objective identification, Precipitation intensity, Cyclone classification

Introduction

Extratropical cyclones (ECs) and their associated fronts are the most important weather systems for the precipitation in mid-latitudes. Some studies found that in many regions, including parts of Europe and much of North America, over 70% of total precipitation is associated with ECs (Harvey et al. 2012). As one of the areas with most frequent EC activities, East Asia is also strongly affected by ECs (Chang 2005; Adachi and Kimura 2007; Lee et al. 2020). The impact of cyclone movement and development often extends from East Asian continent to the Northwest Pacific Ocean. Moreover, the cyclone activity is often accompanied by some meteorological phenomena, such as strong precipitation and gale, which may bring serious social losses (Chen et al. 2017; Bentley et al. 2019). For example, on December 16, 2014, a deep trough with high potential vorticity (PV) reached over the East China Sea west of Japan made an EC build and the low-level moisture strengthen. The water vapor was transported toward the coastal region by the cyclone, which caused a record-breaking heavy rain during March and April at Owase (Tochimoto and Iizuka

*Correspondence:
Yujing Qin
qinyujing@nuist.edu.cn
Chuhan Lu
luchuhan@nuist.edu.cn
[1] Key Laboratory of Meteorological Disaster, Ministry of Education/Joint International Research Laboratory of Climate and Environment Change/Collaborative Innovation Center on Forecast and Evaluation of Meteorological Disasters, Nanjing University of Information Science and Technology, 219 Ningliu Road, Nanjing 210044, China
[2] Key Laboratory of Ecosystem Carbon Source and Sink, China Meteorological Administration (ECSS-CMA), Wuxi University, 214063 wuxi, China

2022). Therefore, it is important to study the relationship between ECs and regional-scale precipitation extremes under present-day climate conditions in an event-based manner.

The structure and intensity of ECs have great influence on the EC-related precipitation intensity. Hawcroft et al. (2012) documented that the proportion of precipitation caused by ECs increases obviously with the increase of cyclone intensity, and the strongest 10% of ECs in summer account for about 20% of the total EC-related precipitation, while the weakest 20% contribute only 4% of the total precipitation. The ECs related to extreme precipitation have larger intensity, longer duration, and larger average wind speed (Reale et al. 2019; Owen et al. 2021). However, in the analysis of the cyclone properties that are related to heavy precipitation, Stephan and Land (2012) found that the ECs related to heavy precipitation are only stronger at the exit of the path and have no difference with other cyclones in their formation and strengthening processes. The ECs associated with heavy precipitation in much of the Northern Hemisphere, such as on the eastern flank of the continents and at the entrance of the Northern Hemisphere storm tracks, have a more equatorward origin (Stephan and Heini 2012), which may be related to the water vapor conditions required for heavy precipitation.

However, compared with the existing abundant classification methods of tropical cyclones, the definition and classification of EC intensity are limited due to their relatively complex shape and structure by selecting one-dimensional physical quantities to characterize cyclone intensity (Zhang et al. 2018; Hunter et al. 2016; Yu et al. 2020; Felker et al. 2010). The objective identification method we used can improve the recognition of the complex structure and evolution of ECs. Therefore, the relationship between EC-associated meteorological factors and precipitation is analyzed in this study by using the cyclone zone identification method. Moreover, the ECs are classified based on a newly defined EC intensity, so as to provide clues for the prediction of EC-associated precipitation intensity through the monitoring and forecasting on different levels of cyclones.

The remainder of this paper is organized as follows. "Data and method" section presents the data and method used in this study. The effects of ECs on the precipitation over East Asia in summer are investigated in "Effects of ECs on the precipitation over East Asia in summer" section. The EC classification is discussed in "Cyclone classification" section. The conclusion and a brief discussion are given in "Conclusions and discussion" section.

Data and method

Data

The data used in this study are in the summers (June–August) of 1979–2018. The ERA-Interim (Dee et al. 2011) 6-h geopotential height dataset at 850 hPa (Z850) with a relative high resolution (~0.7° * 0.7°, N128 grid) are chosen to detect cyclone zones. The reason we chose Z850 for EC detection is because the geopotential height is mass field, using this variable allows to consider well-organized surface pressure system, and this area can be considered as the region where EC-related precipitation could occur. We also check the spatial consistency by comparing the location of cyclone center on 850 hPa and the location of minimum SLP within this EC zone. We found that over 53.3% (72.3%) of the above two locations are within 150 km (250 km), showing highly spatial consistency of cyclone center detected in Z850 and SLP. Therefore, we select the Z850 field to detect EC over East Asia in our study.

The best track dataset of tropical cyclones comes from the Tropical Cyclone Data Center of the China Meteorological Administration (https://tcdata.typhoon.org.cn), which is used to exclude the impact of tropical cyclone. The data include the location and intensity of tropical cyclones every 6 h (Ying et al. 2014; Lu et al. 2021).

Method

A cyclone identification method is designed to detect the cyclone zone (e.g., Hodges 1994; Simmonds 2000; Wang et al. 2009; Dacre et al. 2020; Okajima et al. 2021). The method is based on the outermost closed contour scheme improved by Lu (2017, here after LU17) and Lu et al. (2020). In particular, a cyclone-center candidate is determined as the Z850 grid point that is lower than all eight surrounding grid points on a latitude–longitude grid mesh, and 4 gpm is used as the contour interval for enclosed contour searching. If the contour is closed, a cyclone is identified, and the area surrounded by the outermost contour is taken as the influence area of the cyclone. This method is capable of identifying the two-dimensional cyclone region and is not limited by cyclone lifetime (Neu et al. 2013).

By considering whether there are several centers sharing a common outmost enclosed contour, the method can capture the merging cases of separated cyclones or the splits from multicenter cyclone. It is noted that the splitting and merging could increase the uncertainty of cyclone tracking. For example, LU17 reported that a merge of two cyclones origin from the Siberia and local Arctic Ocean, respectively, can lead to two different tracks of the Great Arctic Cyclone of August 2012 when using different tracking methods. And he found that the cyclone from local Arctic Ocean dramatically intensified

the one from Siberia when they merged (C.F. Figure 3 in LU17); therefore, the merge case is identified and a different origin of this extreme cyclone is shown by LU17's algorithm.

This study firstly identifies the summer ECs in East Asia (23.5° N–66.5° N, 60° E–150° E). When the EC influences area falls into East Asia, it is considered as an EC affecting East Asia. Since some cyclones in the temperate zone are northward-moving tropical cyclones, we compared the location of our cyclone center with the one, if exists, in the best track of TCs from China Meteorological Administration in the same date and time. If the two locations are within one grid point distance (~78 km), the identified cyclone from ERA-interim is considered as a TC and excluded from our EC dataset. Finally, 6225 TCs are removed. As the influence of cyclones has a certain time scale, the running mean value of precipitation within ±12 h is taken as the cyclone-associated precipitation for a given time step. This method results in a higher correlation between cyclones and precipitation than the corresponding 6-h precipitation.

Effects of ECs on the precipitation over East Asia in summer

To explore the influence of ECs on local precipitation, Fig. 1a and b presents the scatter plots of the spatial mean depth and central wind speed (which are traditionally considered as the EC intensity) to the maximum precipitation ($R_{\max}$) within ±12 h in the cyclone area. Considering MSLP or Z850 may be affected by large spatial scales (Hoskins and Hodges 2002), we define a cyclone mean depth in a spatially smoothed way which is the average of the difference between Z850 in each grid with the EC and the central $Z850(\frac{1}{n}\sum_{i=1}^{n}(Z_i - Z_{\min}))$. As can be seen, a weak negative correlation is found between the spatial mean depth and $R_{\max}$ (the correlation coefficient is only 0.38). Compared with the spatial mean depth, the correlation coefficient between the wind speed of central point (denoted by the average of 9 adjacent grids) and $R_{\max}$ pronouncedly increase ($r = 0.57$).

The horizontal distributions of divergence, pressure gradient, and water vapor condition within an EC regime also make substantial contribution to its associated precipitation intensity. For example, Pfahl and Sprenger (2016) found that cyclone intensity is more closely

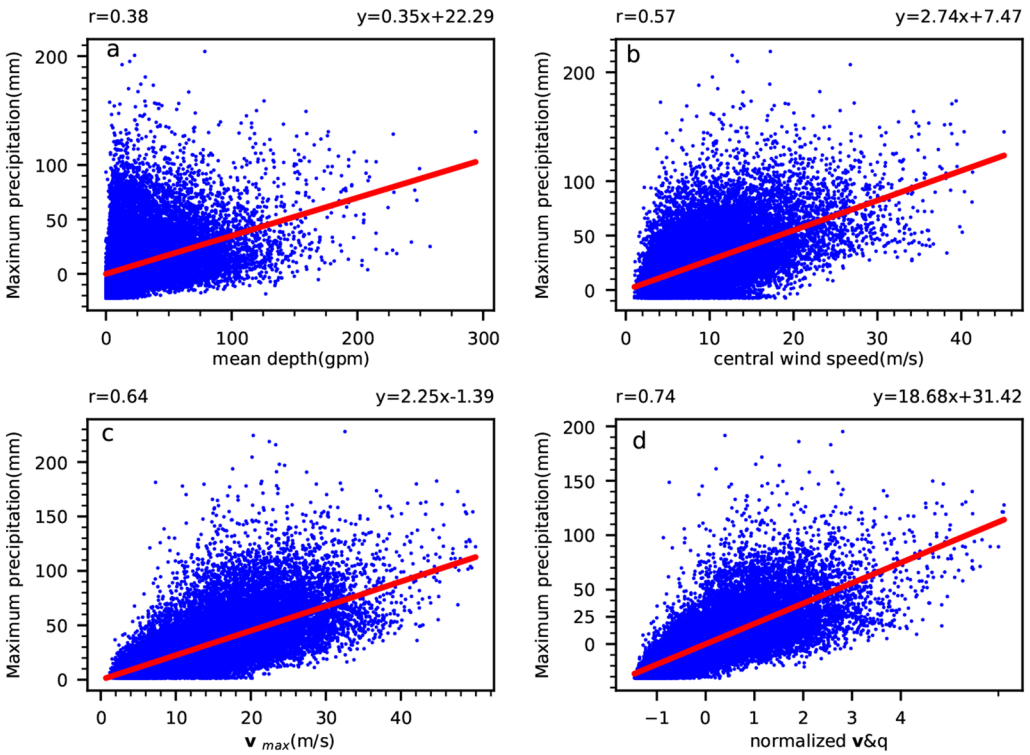

Fig.1 Scatter plots between the 6 hourly maximum precipitation within ±12 h ($R_{\max}$) and the **a** mean depth, **b** central wind speed, **c** maximum wind speed ($v_{\max}$) and **d** maximum product of the normalized wind speed and specific humidity ($vq_{\max}$) within the corresponding EC region in East Asia in the summers from 1979 to 2018. The linear fitting line is marked by a red solid line. All these correlations statistically pass the significance of 0.01 Monte Carlo simulations test

related to the frequency and intensity of extreme precipitation within its two-dimensional cyclone area (Wernli and Schwierz 2006), which is identified as the finite area that surrounds a local SLP minimum and is enclosed by the outermost closed SLP contour. Therefore, the scatter distribution and linear fitting of maximum wind speed (v_{max}) and R_{max} in the cyclone area are shown in Fig. 1c. The correlation coefficient between them reaches 0.64, and the significance of correlation is higher than the relationship between R_{max} and the EC central geopotential height. As the v_{max} increases, the intensity of EC-associated R_{max} increases obviously, suggesting a dynamically driven role of horizontal wind on R_{max} that may be linked with enhanced vertical motion and water vapor transportation. As documented by Dacre et al. (2019), the branch of the cyclone-relative airflow toward the cyclone center within a cyclone's warm sector supplies moisture to the base of the warm conveyor belt where it ascends and precipitation form, explaining the link between atmospheric rivers and the precipitation associated with warm conveyor belt.

It should be pointed out that in addition to the dynamic conditions, the abundance of water vapor is also a key factor affecting precipitation. Therefore, considering the water vapor condition at the grid where the maximum wind speed is located, both (u, v) and q on the 850 hPa level are used to calculate the vq_{max}. The vq_{max} is defined as follows:

$$\begin{cases} vq_i = \sqrt{(u_i q_i)^2 + (v_i q_i)^2} \\ vq_{\max} = \mathrm{MAX}\left(\dfrac{vq_i - \overline{vq_i}}{\frac{1}{n}\sum_{i=1}^{i=n} \sqrt{(vq_i - \overline{vq_i})^2}} \right) \end{cases}.$$

The vq_{max} is tried to find the maximum normalized moisture flux on the 850 hPa within each individual cyclone. In particular, the normalization is done for the value of water vapor flux $\sqrt{(u_i q_i)^2 + (v_i q_i)^2}$. $\overline{vq_i}$ is the average value of the product of wind speed and specific humidity at all grid points in the cyclone region. The vq_{max} indicates an intensity of EC-associated moisture flux in the lower troposphere and is used to explore how the EC affect the regional rainfall. Figure 1d shows the scatter distribution of vq_{max} on 850 hPa to the maximum precipitation. It is shown that compared to other traditional $1 - D$ intensify of EC, such as center SLP and wind speed in the central areas, a most significant positive correlation is shown between the vq_{max} and the maximum precipitation ($r = 0.74$). Consistently, the correlation coefficients between R_{max} and vq_{max} from vertically integrated moisture flux ($r = 0.74$, as shown in Additional file 1: Fig. S1). This indicates that vq_{max} can be the most relevant to active precipitation around an EC, which can be a good indicator for the cyclone-related maximum precipitation. The above results are also checked by using ERA5 reanalysis data, and a high consistency is supplemented and shown in Additional file 2: Fig. S2.

To study the spatial distribution and connection of vq_{max} and R_{max}, Fig. 2 shows the spatial distribution

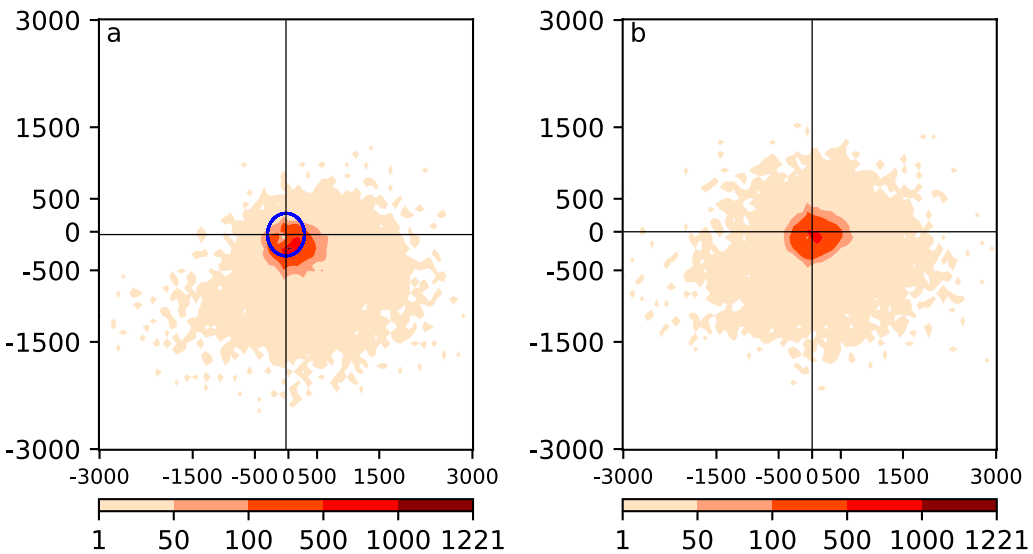

Fig. 2 Frequency distribution of **a** vq_{max} and **b** R_{max} relative to the cyclone center point. (The blue line is a circle with a radius of 300 km away from the cyclone center point)

frequencies of vq_{max} and R_{max} within the cyclone center regime. It can be seen that the high-value areas of vq_{max} and R_{max} spread and gradually decrease outward from the center point, and a large part of them present within the EC central region (radius < 300 km). The proportion of vq_{max} (R_{max}) within 300 km of EC center is 42.6% (45.9%), with a highly spatial consistency. It should be noted that the vq_{max} high-value area is biased toward the south-east quadrant. The reason may be that the prevailing East Asian summer monsoon leads to the strong transport and convergence of water vapor in the southern part of cyclone. A certain part of ECs shows a good spatial coincidence between locations of vq_{max} and maximum EC-related precipitation. In particular, the proportion of their distance less than 3 grid points (~250 km) is over 38.5%. However, the location of vq_{max} indicates a maximum low-level moisture flux could not well represent the position of maximum EC-related precipitation. The latter could be more linked with the maximum convergence of vertical-integrated moisture flux.

Cyclone classification

EC classification and its relationship with precipitation

Because of the irregular shapes of ECs, especially in inland areas, traditional auto-detecting methods mainly focus on the cyclone center identification or considering a given value as its radius (Raible et al. 2007). Meanwhile, the above results show that both vq_{max} and R_{max} are mainly distributed in the central region. To simplify the definition of intensity index and improve the operational monitoring efficiency, the vq_{max} in the central region (vq_{max_300}) is taken as the cyclone overall intensity index. The correlation coefficient between vq_{max} and vq_{max_300} is 0.87, showing a good consistency. As shown in Fig. 3a, vq_{max_300} still maintains an evident positive correlation with R_{max} (correlation coefficient: 0.7). To explore how the EC affect the regional rainfall, we classify these EC into certain level based on the vq_{max300}. According to the Chinese National Standards GB/T 28592-2012 Grade of precipitation, the rain rate intensity can be divided into four grades (light rain: 0–10 mm/day; moderate rain: 10–25 mm/day; heavy rain: 25–50 mm/day; down pour: > 50 mm/day). Accordingly, we also classify the EC into four levels base on the vq_{max_300}. As shown in Fig. 3b and c, the EC level with the largest probability increases with the upgrade of precipitation level. Specifically, when $vq_{max\_300} < -0.58$, the probability of light rain is 26.9%; when $-0.17 > vq_{max\_300} \geq -0.58$, the probability of moderate rain is 88.3%; when $0.51 > vq_{max\_300} \geq -0.17$, the

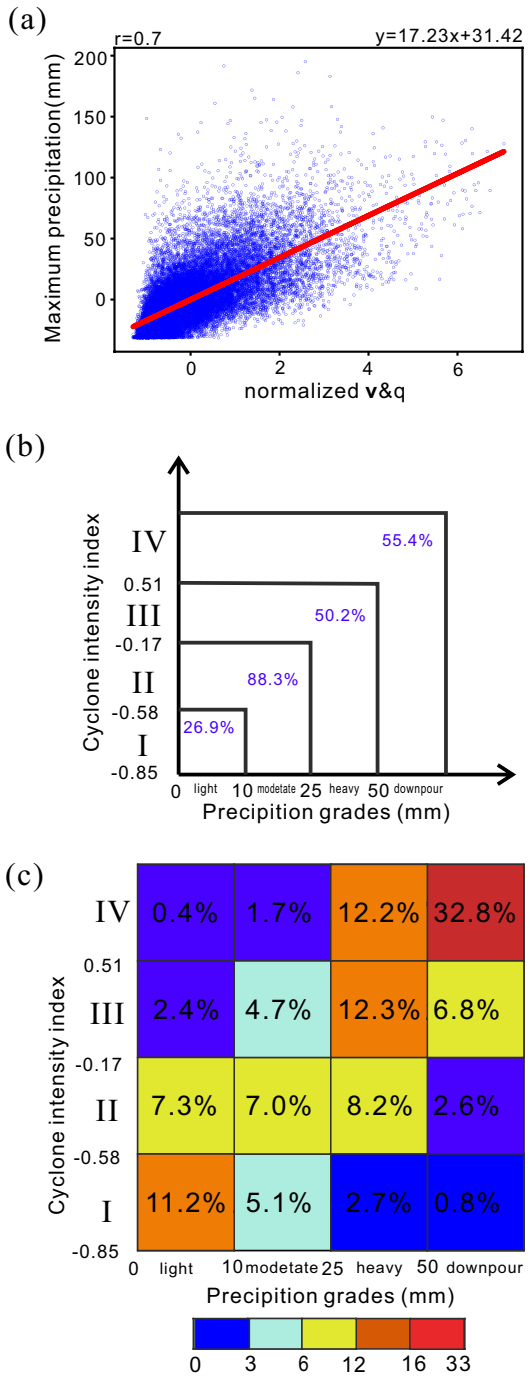

Fig. 3 Scatter plots between the 6 hourly vq_{max_300} and the ± 12-h maximum precipitation in the cyclone area (**a**) (The correlation statistically pass the significance of 0.01 Monte Carlo simulations test); Dependence of precipitation events on EC in different grades (**b**); The probability of different levels EC when different levels precipitation occurred (**c**). The linear fitting line is marked by a red solid line in (**a**)

probability of heavy rain is 50.2%; when $vq_{max\_300} \geq 0.51$, the probability of rainstorm is 55.4%. Therefore, according to the value of vq_{max_300}, the ECs are grouped into four levels as follows: I: $vq_{max\_300} < -0.58$; II: $-0.17 > vq_{max\_300} \geq -0.58$; III: $0.51 > vq_{max\_300} \geq -0.17$; and IV: $vq_{max\_300} \geq 0.51$.

To further show the relationship between different levels of ECs and the associated maximum precipitation, Fig. 3c demonstrates the probability of different levels of ECs when different levels of precipitation occurs. It can be seen that the EC level with the largest probability increases with the increase of precipitation level. More importantly, 32.8% of summer heavy rain events in East Asia are related to level-4 EC. James et al. (2018) also reported that the largest precipitation occurs more often when the cyclones are the strongest dynamically. Based on the above analysis, it is reasonable to divide the summertime East Asia ECs into four intensity levels according to the value of vq_{max_300}, which can well indicate the associated maximum precipitation.

Cases and evolution of level-4 ECs with different horizontal scales

As mentioned earlier, heavy precipitation events are often associated with level-4 ECs, but the horizontal scales of these strong cyclones vary widely. In the past 40 years, there have been 3435 level-4 ECs accompanied by heavy rain. To record the horizontal extent (zone) of the multiscale cyclones, a circular area equal to the area of the grid points covered by closed contours around the periphery is considered, and the radius of the circle is treated as the equivalent radius of the cyclone. Among these level-4 ECs, the frequencies of EC_I (radius < 150 km), EC_{II} (150 km < radius < 500 km), and EC_{III} (radius > 500 km) are 0.44%, 48.47% and 51.09%, respectively. This indicates that the EC that breeds heavy precipitation does not necessarily have a large horizontal scale, and some heavy precipitation may come from EC_{II} or even EC_I (local low vortex). To further reveal the differences of horizontal scales of level-4 ECs, Fig. 4 shows three level-4 ECs with different horizontal scales, which are all associated with heavy precipitation. The first case (Fig. 4a) shows that at 1800 UTC on July 4, 2013, a long and narrow rain belt appeared in the Huanghuai River Basin, and the largest precipitation occurred in southern Shandong Peninsula and the Yellow Sea. This event was accompanied with an EC_I vortex on the Meiyu front. It can be clearly seen that the southwesterly air flow continuously transported water vapor, and the maximum region of vertically integrated moisture transport flux convergence and the notable ascending area located near the rain belt (Fig. 4d). The shear line at the lower troposphere dynamically facilitates

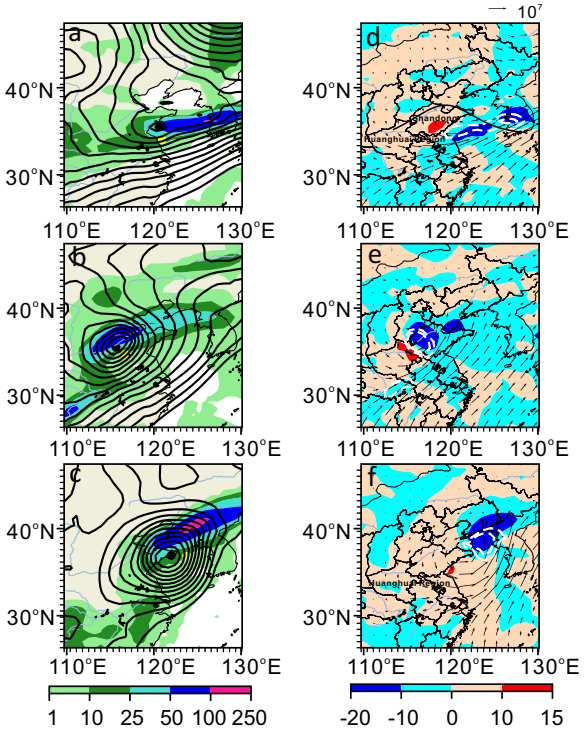

Fig. 4 Precipitation (shades, unit: mm day^{-1}) and geopotential height (contour, unit: gpm) fields in three EC cases with different horizontal scale at **a** 1800 UTC on July 4, 2013, **b** 0000 UTC on June 26, 2005 and **c** 0600 UTC on July 25, 2014. The black dots show the cyclone center point. The yellow dots show the location of vq_{max}. The distribution of vertically integrated water vapor flux (black vector, unit: g m^{-1} s^{-1}) and its divergence (shades, unit: g m^{-2} s^{-1}) and vertical motion (white contours denote the values of − 0.5, − 1 Pa s^{-1}) (**d**–**f**). The black line in **d** is a Meiyu front adapted from JMA (https://www.data.jma.go.jp/fcd/yoho/data/hibiten/2013/1307.pdf)

the upward motion and water vapor convergence. The analysis of the 850 hPa geopotential height suggests that the EC_I cyclonic circulation is embedded from northeast to southwest in the low trough over southern Shandong Peninsula. Although the horizontal scale of this cyclone is relatively small (radius = 144 km), the 24-h accumulated precipitation associated with it can reach the rainstorm level (R_{max} = 96.25 mm). During this period, the maximum wind speed in the cyclone reached 26.7 m/s, accompanied with a favorable water vapor condition (the specific humidity value at the maximum wind speed point is 15.2 g/kg). The vq_{max_300} index is up to 2.92, so it is considered as a level-4 EC with heavy precipitation.

The second case (Fig. 4b) is an EC at EC_{II} scale (radius = 458.8 km) which caused a heavy precipitation event in East China at 0000 UTC on June 26, 2005. The EC was a typical Huanghuai cyclone. It was generated in the Sichuan Basin (28°–32° N, 105°–110° E) with a cold core. The cold air carried by the EC from the mid- and

high latitudes converged with the southwesterly warm-humid airflow carried by the East Asian monsoon, inducing pronounced precipitation in East China and northern South China. The maximum precipitation was located in the northern part of the cyclone in North China, with a value of 105.5 mm. The EC maximum wind speed was 25.1 m/s, and the corresponding specific humidity value was 15.8 g/kg, indicating that the EC carried large kinetic energy and water vapor. The $vq_{\max\_300}$ index value is 2.82, which satisfies the criteria of level-4 EC.

The third case (Fig. 4c) occurred at 0600 UTC on July 25, 2014, and it was a heavy rain event caused by an EC_{III} cyclone. The 24-h accumulated maximum precipitation reached the rainstorm level. The EC was also formed in Southwest China, and it moved northeastward and continuously deepened. When it reached Huanghuai region, it connected with the western Pacific subtropical high. As a result, the zonal land–sea pressure gradient between them was intensified (figure not shown), which was favorable for the strengthening of the southwesterly warm-humid airflow, and provided abundant water vapor for the rainstorm. The maximum precipitation area was located in Northeast China, and the 24-h accumulated maximum precipitation reached 114.1 mm. The maximum wind speed reached 25.1 m/s, and the corresponding specific humidity value was 15.8 g/kg. The $vq_{\max\_300}$ index is 2.87, which is a level-4 EC. It can be seen that pronounced convergence area with notable ascending is well consistent with the regions where heavy rainfall occurred (Fig. 4d–f).

To analyze the evolution and differences of the $vq_{\max\_300}$ between the EC_{II} and EC_{III}, Fig. 5 shows the evolution of the 50 strongest $vq_{\max\_300}$ cyclones during their life cycles. The proportions of these two scales level-4 ECs are both 50%. As shown in Fig. 5a, most of the EC_{II}-scale cyclones develop rapidly during their early stages. In particular, for 52% of the cases the $vq_{\max\_300}$ reaches the peak in the first 24 h. Then, the intensity gradually decreases from 24 to 72 h, and a small part (24%) of the EC_{II} can live over 72 h. Compared with the EC_{II}, the EC_{III} develops more slowly, with an average $vq_{\max\_300}$ value of 3.81, slightly larger than that of the EC_{II} (3.51). However, only five ECs reach the strongest in the first 24 h, and 48% of ECs reach their strongest intensity at around 24–36 h. Then, they gradually weaken from 36 to 90 h. Some of them could even last for more than 90 h (Fig. 5b). During the evolution of these two scales of ECs, the maximum intensity mostly appears in the early stage (72% of EC_{II} and 52% of EC_{III}), which is consistent with the result revealed by Martina and Simmonds (2021) that the extreme wind speed and precipitation are more likely to appear before the cyclone half-life time. In general, compared with EC_{II}, the EC_{III} has a relatively higher maximum vq_{max_300} and a longer duration.

Conclusions and discussion

The ECs have been extensively studied. The methods used for classification have been applied to study their dynamic characteristics and contribute to the forecasting of these systems (Gushchina et al. 2008; Catto 2016; Bieli et al. 2019). By using a two-dimensional EC objective identification method, the summertime East Asian EC dataset is obtained. Then, the intensity of ECs is investigated. Based on the maximum wind speed and water vapor conditions in the EC regime, we define and classify the EC intensity. Moreover, the relationship between EC and the associated precipitation is investigated in detail. The main conclusions are as follows.

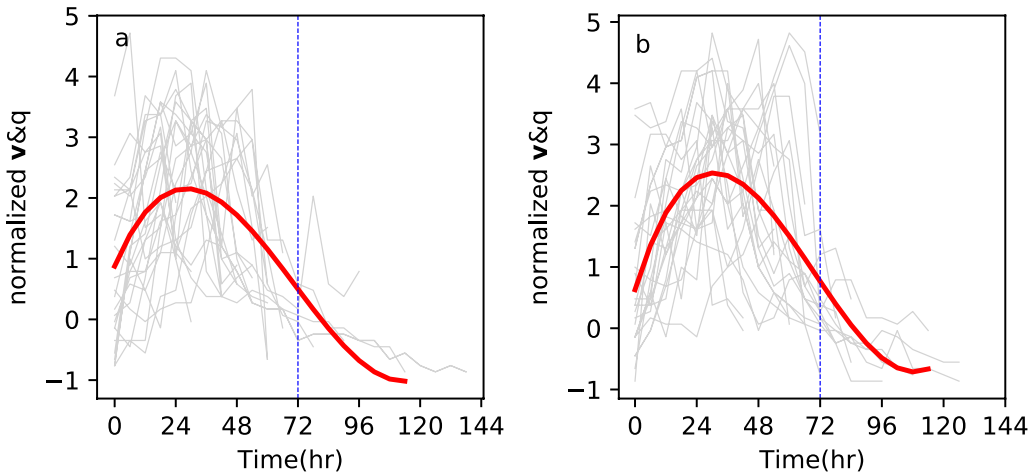

Fig. 5 Evolution of the $vq_{\max\_300}$ among the 50 strongest level-4 EC in EC_{II} (**a**) and EC_{III} (**b**) scale. The red line is the cubic regression fitting curve; the blue dotted line corresponds to 72 h

Different from the traditional definition of EC intensity by the central pressure or central wind speed, in this study we define the cyclone intensity index (vq_{max}) as the maximum product of wind speed and the corresponding specific humidity in the cyclone regime. This index is most closely related to the relevant 24-h maximum precipitation, with a correlation coefficient of 0.74. Based on the simplified intensity index (vq_{max_300}), ECs are categorized into four levels. As the EC level increases, its corresponding precipitation intensity also increases obviously. 32.8% of the heavy precipitation events in East Asian summer are associated with level-4 EC (the strongest group). Among all the level-4 ECs, the frequencies of EC_I (radius < 150 km), EC_{II} (150 km < radius < 500 km), and EC_{III} (radius > 500 km) are 0.44%, 48.47%, and 51.09%, respectively. Seen from the evolution of the strongest 50 level-4 ECs, the peak of synoptic-scale ECs generally lags behind that of EC_{II}, and the largest vq_{max_300} of EC_{III} is slightly higher than that of EC_{II}.

In this study, the East Asian summer ECs are classified based on the relationship between ECs and precipitation intensity, but the effects of ECs on precipitation in different stages are different (Zhang et al. 2020), which may be related to the complex interaction of multiple factors within the cyclone mesoscale substructure (William et al. 1976). Therefore, the relationship between ECs and precipitation requires further research.

Abbreviations

R_{max}	± 12-Hour maximum precipitation (R_{max}) in the cyclone area
V_{max}	Maximum wind in the cyclone area
vq_{max}	The maximum value of the product of the normalized wind speed and the specific humidity

Supplementary Information

The online version contains supplementary material available at https://doi.org/10.1186/s40562-023-00267-w.

Additional file 1: Fig. S1. The relationship between vq_{max} derived from the vertical-integrated moisture flux and maximum precipitation within ± 12 h (R_{max}) in East Asian summer from 1979 to 2018.

Additional file 2: Fig. S2. The relationship between the central geopotential (a), central wind speed (b), maximum wind speed (c), and the normalized maximum product of wind speed and specific humidity in cyclone region and R_{max} in East Asian summer from 1979 to 2018 from ERA5 data.

Acknowledgements
The authors would like to thank Kong Yang for his helpful suggestions and useful datasets. The authors express their appreciation of the staff at ECMWF for making the reanalysis datasets freely available.

Author contributions
STW and YJQ conceived the study. STW wrote the initial manuscript in discussion with YJQ. STW contributed to the data analysis and produced figures. CHL improved the manuscript. ZYG provided many good suggestions for the article. All the authors contributed to interpreting results, discussion, and revision of this paper. All the authors read and approved the final manuscript.

Funding
This work was jointly sponsored by Key R & D plan of Jiangsu Province (Grant No. BE2022161), the National Key Research and Development Program of China (Grant No. 2019YFC1510201), and the National Natural Science Foundation of China (Grant Nos. 41975073).

Availability of data and materials
The geopotential height dataset to capture the cyclone can be found at https://www.ecmwf.int/en/forecasts/datasets/reanalysis-datasets/era-interim. The precipitation, specific humidity, and wind speed also come from here. The best track dataset of tropical cyclones used in this paper comes from the Tropical Cyclone Data Center of the China Meteorological Administration (https://tcdata.typhoon.org.cn).

Declarations

Competing interests
The authors declare no conflicts of interest in this work.

Received: 10 August 2022 Accepted: 14 February 2023
Published online: 07 March 2023

References

Adachi SA, Kimura F (2007) A 36-year climatology of surface cyclogenesis in East Asia using high-resolution reanalysis data. Sola 3:113–116
Bentley AM, Bosart LF, Keyser D (2019) A climatology of extratropical cyclones leading to extreme weather events over central and eastern North America. Mon Weather Rev 147:1471–1490. https://doi.org/10.1175/MWR-D-18-0453.1
Bieli M, Camargo SJ, Sobel AH, Evans JL, Hall T (2019) A global climatology of extratropical transition. Part II: statistical performance of the cyclone phase space. J Clim 32:3583–3597. https://doi.org/10.1175/JCLI-D-18-0052.1
Catto JL (2016) Extratropical cyclone classification and its use in climate studies. Rev Geophys 54:486–520. https://doi.org/10.1002/2016RG000519
Chang EKM (2005) The impact of wave packets propagating across asia on pacific cyclone development. Mon Weather Rev 133(7):1998–2015. https://doi.org/10.1175/MWR2953.1
Chen HS, Teng FD, Zhang WX, Liao H (2017) Impacts of anomalous midlatitude cyclone activity over East Asia during summer on the decadal mode of East Asian summer monsoon and its possible mechanism. J Clim 30(2):739–753. https://doi.org/10.1175/JCLI-D-16-0155.1
Dacre R, Helen F et al (2019) Linking atmospheric rivers and warm conveyor belt airflows. J Hydrometeorol 20:1183–1196
Dacre HF, Josey SA, Grant AL (2020) Extratropical-cyclone-induced sea surface temperature anomalies in the 2013–2014 winter. Weather Clim Dyn 1(1):27–44
Dee DP, Uppala SM, Simmons AJ, Berrisford P, Poli P, Kobayashi S, Andrae U, Balmaseda MA, Balsamo G, Bauer P, Bechtold P, Beljaars ACM, van de Berg L, Bidlot J, Bormann N, Delsol C, Dragani R, Fuentes M, Geer AJ, Haimberger L, Healy SB, Hersbach H, Holm EV, Isaksen L, Kallberg P, Kohler M, Matricardi M, McNally AP, Monge-Sanz BM, Morcrette JJ, Park BK, Peubey C, de Rosnay P, Tavolato C, Thepaut JN, Vitart F (2011) The ERA-Interim reanalysis: configuration and performance of the data assimilation system. Q J Roy Meteorol Soc 137:553–597. https://doi.org/10.1002/Qj.828
Felker SR, LaCasse B, Tyo S, Ritchie EA (2010) Forecasting post-extratropical transition outcomes for tropical cyclones using support vector machine classifiers. J Atmos Oceanic Tech 28:709–719. https://doi.org/10.1175/2010JTECHA1449.1
Gushchina DY, Arakelyan TG, Petrosyants MA (2008) The relation between circulation intensity in the temperate latitude cyclone and air temperature

and precipitation anomalies. Russ Meteorol Hydrol 33:681–691. https://doi.org/10.3103/S1068373908110010
Harvey BJ, Shaffrey LC, Woollings TJ, Zappa G, Hodges KI (2012) How large are projected 21st century storm track changes? Geophys Res Lett 39:L18707. https://doi.org/10.1029/2012GL052873
Hawcroft MK, Shaffrey LC, Hodges KI, Dacre HF (2012) How much Northern Hemisphere precipitation is associated with extratropical cyclones? Geophys Res Lett 39:L24809. https://doi.org/10.1029/2012GL053866
Hodges K (1994) A general method for tracking analysis and its application to meteorological data. Mon Weather Rev 122:2573–2586. https://doi.org/10.1175/1520-0493(1994)122,2573:AGMFTA.2.0.CO;2
Hoskins BJ, Hodges KI (2002) New perspectives on the Northern Hemisphere winter storm tracks. J Atmos Sci 59(6):1041–1061
Hunter A, Stephenson DB, Economou T, Holland M, Cook I (2016) New perspectives on the collective risk of extratropical cyclones. Q J R Meteorol Soc 142(694):243–256. https://doi.org/10.1002/qj.2649
James F, Booth Catherine M, Naud Jeyavinoth, Jeyaratnam (2018) Extratropical Cyclone Precipitation Life Cycles: A Satellite Based Analysis. Geophys Res Lett 45(16):8647–8654. https://doi.org/10.1029/2018GL078977
Lee J, Son SW, Cho HO, Kim J, Cha DH, Gyakum JR, Chen D (2020) Extratropical cyclones over East Asia: climatology, seasonal cycle, and long-term trend. Clim Dyn 54(1):1131–1144
Lu CH (2017) A modified algorithm for identifying and tracking extratropical cyclones. Adv Atmos Sci 34(07):909–924. https://doi.org/10.1007/s00376-017-6231-2
Lu C, Kong Y, Guan Z (2020) A mask R-CNN model for reidentifying extratropical cyclones based on quasi-supervised thought. Sci Rep 10:15011. https://doi.org/10.1038/s41598-020-71831-z
Lu XQ, Yu H, Ying M, Zhao BK, Zhang S, Lin LM, Bai LN, Wan RJ (2021) Western North Pacific tropical cyclone database created by the China Meteorological Administration. Adv Atmos Sci 38(4):690–699. https://doi.org/10.1007/s00376-020-0211-7
Martina M, Simmonds I (2021) Global analysis of cyclone-induced compound precipitation and wind extreme events. Weather Clim Extrem 32:100324. https://doi.org/10.1016/j.wace.2021.100324
Neu U et al (2013) IMILAST: a community effffort to intercompare extratropical cyclone detection and tracking algorithms. Bull Am Meteorol Soc 94:529–547
Okajima S, Nakamura H, Kaspi Y (2021) Cyclonic and anticyclonic contributions to atmospheric energetics. Sci Rep 11(1):1–10
Owen LE, Catto WL, Stephenson DB, Dunstone NJ (2021) Compound precipitation and wind extremes over Europe and their relationship to extratropical cyclones. Weather Clim Extrem 33(1):100342. https://doi.org/10.1016/j.wace.2021.100342
Pfahl S, Sprenger M (2016) On the relationship between extratropical cyclone precipitation and intensity. Geophys Res Lett 43:1752–1758. https://doi.org/10.1002/2016GL068018
Raible CC, Yoshimori M, Stocker TF, Casty C (2007) Extreme midlatitude cyclones and their implications for precipitation and wind speed extremes in simulations of the Maunder Minimum versus present day conditions. Clim Dyn 28:409–423. https://doi.org/10.1007/s0382-006-0188-7
Reale M, Liberato ML, Lionello P, Pinto JG, Salon S, Ulbrich S (2019) A global climatology of explosive cyclones using a multi-tracking approach. Tellus 71A:1611340. https://doi.org/10.1080/16000870.2019.1611340
Simmonds I (2000) Size changes over the life of sea level cyclones in the NCEP reanalysis. Mon Weather Rev 128:4118–4125. https://doi.org/10.1175/1520-0493(2000)129%3c4118:SCOTLO%3e2.0.CO;2
Stephan P, Heini W (2012) Quantifying the relevance of cyclones for precipitation extremes. J Clim 25(19):6770–6780. https://doi.org/10.1175/JCLI-D-11-00705.1
Tochimoto E, Iizuka I (2022) Impact of warm sea surface temperature over a Kuroshio large meander on extreme heavy rainfall caused by an extratropical cyclone. Atmos Sci Lett. https://doi.org/10.1002/asl.1135
Wang XM, Zhai PM, Wang CC (2009) Variations in extratropical cyclone activity in northern East Asia. Adv Atmos Sci 26:471–479. https://doi.org/10.1007/s00376-009-0471-8
Wernli H, Schwierz C (2006) Surface cyclones in the ERA-40 dataset (1958–2001). Part I: novel identification method and global climatology. J Atmos Sci 63:2486–2507. https://doi.org/10.1175/JAS3766.1
William RCB, George S, Heevera VD (1976) Mesoscale rainbands in extratropical cyclones. Mon Weather Rev 104(7):868–878. https://doi.org/10.1175/15200493(1976)104%3c0868:MRIEC%3e2.0.C0;2
Ying M, Zhang W, Yu H, Lu X, Feng J, Fan Y, Zhu Y, Chen D (2014) An overview of the China Meteorological Administration tropical cyclone database. Atmos Ocean Technol 31:287–301. https://doi.org/10.1175/JTECH-D-12-00119.1
Yu B, Wang XL, Yang F, Chan R, Compo GP, Slivinski LC, Sardeshmukh PD, Wehner M, Yang XY (2020) Northern Hemisphere Extratropical Cyclone Activity in the Twentieth Century Reanalysis Version 3 (20CRv3) and its relationship with continental extreme temperatures. Atmosphere 13(8):1166. https://doi.org/10.3390/atmos13081166
Zhang ZH, Martin R, Zhang MH (2018) The relationship between extratropical cyclone strength and atmospheric river intensity and position. Geophys Res Lett 46(3):1814–1823
Zhang A, Chen Y, Zhang X, Zhang Q, Fu Y (2020) Structure of Cyclonic Precipitation in the Northern Pacific Storm Track Measured by GPM DPR. J Hydrometeorol 21(2):227–240

Publisher's Note